ATLAS NOTE

ATLAS-CONF-2013-011

March 5, 2013

Search for invisible decays of a Higgs boson produced in association with a Z boson in ATLAS

The ATLAS Collaboration

Abstract

A direct search for evidence of decays to invisible particles of a Higgs boson at the Large Hadron Collider is presented. This search is performed for a Standard Model-like Higgs boson produced in association with a Z boson and having a mass between $m_H = 115$ GeV and $m_H = 300$ GeV. The results are interpreted to place limits on the branching fraction to invisible particles of the newly discovered boson with mass near 125 GeV. Assuming that this is the Standard Model Higgs boson, its decay to invisible particles is not measurable, but could have a large contribution from the decay to the dark matter particles, for example. In addition, limits are set on any neutral Higgs-like particle, produced in association with a Z boson and decaying predominantly to invisible particles.

No deviation from the Standard Model expectation is observed in the search, which uses 4.7 fb^{-1} of 7 TeV pp collision data and 13.0 fb^{-1} of 8 TeV pp collision data collected by the ATLAS experiment at the LHC. Assuming the ZH production rate for a 125 GeV Standard Model Higgs boson, limits are set on the invisible branching fraction at 95% confidence level. The observed exclusion is for branching fractions greater than 65%, and the expected limit is 84%.

ATLAS-CONF-2013-011
06 March 2013

1 Introduction

Some extensions to the Standard Model (SM) allow a Higgs boson [1–3] to decay to stable or long-lived particles that interact with the Higgs boson, but have only weak interactions with other elementary particles. Results obtained so far in the search for the SM Higgs boson do not exclude the possibility of a sizable branching ratio to invisible particles for the SM Higgs boson candidate at $m_H \sim 125$ GeV [4, 5]. Combined LEP results [6] have excluded an invisibly decaying Higgs boson for $m_H < 114.4$ GeV under the assumption that such a Higgs boson is produced in association with a Z boson at the rate expected for a SM Higgs boson and that it decays predominantly to invisible particles. A further Higgs-like boson decaying predominantly to invisible particles is not excluded for $m_H > 115$ GeV. This note presents a search for decays to invisible particles for a narrow scalar boson produced in association with a Z boson with the same cross section as the SM Higgs boson and having a mass between 115 and 300 GeV. The results are also interpreted in terms of the 125 GeV Higgs boson candidate, where the ZH production cross section is taken to be that predicted for a SM Higgs boson.

2 Signal Model and Analysis Overview

The signal process searched for is the associated production of ZH. The Higgs boson is assumed to decay to invisible particles as shown in the Feynman diagram in Figure 1. The Z boson decaying into electrons or muons is considered for this analysis. The SM ZH cross section for $m_H = 125$ GeV is 316 fb at $\sqrt{s} = 7$ TeV and 394 fb at $\sqrt{s} = 8$ TeV [7, 8]. It is calculated at NLO [9] and at NNLO [10] in QCD, and NLO EW radiative corrections [11] are applied. Including the requirement that the Z boson decays to e, μ, or τ reduces these cross sections to 31.9 fb and 39.8 fb respectively. A very small SM contribution to the $ZH \to \ell\ell +$ inv. final state arises when the Higgs boson decays to four neutrinos via two Z bosons. The predicted cross section of this process for $m_H = 125$ GeV is $3.4{\times}10^{-2}$ fb at $\sqrt{s} = 7$ TeV and $4.2{\times}10^{-2}$ fb at $\sqrt{s} = 8$ TeV. The present search is not sensitive to this particular process although it is part of the signal, but instead searches for enhancements of the invisible decay fraction due to physics beyond the Standard Model (BSM).

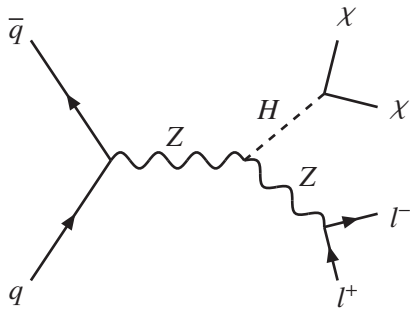

Figure 1: Leading Feynman diagram of the associated ZH production. In this search the Z boson must decay to charged leptons and the Higgs boson must decay to invisible particles which are generically represented by χ.

The POWHEG [12] interfaced with HERWIG++ [13] Monte Carlo (MC) generator is used to simulate the signal. In the simulation the associatively produced Z boson is forced to decay to e, μ, or τ. The invisible decay of the Higgs boson is simulated by forcing the Higgs boson to decay to two Z bosons, which are then forced to decay to neutrinos. For most distributions shown in this note the signal simulation is normalized assuming the SM ZH production rate and a 100% branching fraction of the Higgs boson to invisible particles. Signal samples are generated at Higgs boson masses of 115, 120, 125, 130, 150, 200, and 300 GeV.

This analysis searches for an excess of events over the SM contribution in the dilepton + large missing transverse energy ($E_{\mathrm{T}}^{\mathrm{miss}}$) final states. The processes that contribute to the SM expectation are listed below ordered by the magnitude of their contribution.

- Continuum $ZZ \to \ell\ell\nu\nu$ is irreducible and contributes approximately 70% of the total background.
- $WZ \to \ell\nu\ell\ell$ where the W decay lepton is not identified either by failing lepton identification or by being outside the kinematical selections. The WZ background contributes approximately 20% of the total background.
- Continuum $WW \to \ell\nu\ell\nu$ events where the leptons mimic a Z boson constitute approximately 5% of the background.
- Top quark events ($t\bar{t}$ and Wt) where the leptons mimic a Z boson are considerably reduced by applying a jet veto and contribute approximately 2% of the background.
- Inclusive $Z \to \ell\ell$ events are largely reduced by requiring large $E_{\mathrm{T}}^{\mathrm{miss}}$. Additional cuts are also applied to further suppress this background. The remaining background contributes approximately 1% to the total.
- Inclusive $W \to \ell\nu$ and dijet events can fake the signal if one or two jets are reconstructed as leptons. These backgrounds are approximately 1% of the total.
- $H \to ZZ^{(*)} \to \ell\ell\nu\nu$, for a 125 GeV SM Higgs boson, would produce $E_{\mathrm{T}}^{\mathrm{miss}}$ that falls below the cut. Thus, this process is considered negligible.
- $H \to WW^{(*)} \to \ell\nu\ell\nu$, for a 125 GeV SM Higgs boson, would have a dilepton mass that falls outside the Z peak and is thus also considered to be negligible.

3 Data and Monte Carlo Samples

This search uses 4.7 fb^{-1} of data recorded in 2011 at a center of mass energy of 7 TeV and 13.0 fb^{-1} of data recorded in 2012 at a center of mass energy of 8 TeV. Events are selected using a combination of triggers that select single electrons or muons or a pair of electrons or muons. The trigger efficiency, for signal events passing the full selection cuts described below, is nearly 100% in both data periods in the electron channel, and approximately 95% and 94% in the 2011 and 2012 periods respectively in the muon channel. The data are required to have been recorded during stable beam conditions and during nominal detector performance and data readout conditions.

Background processes are modeled using tree level and NLO MC generators. HERWIG [14] is used to model ZZ, WZ, and WW production for the 2011 data, and SHERPA [15] for the 2012 data. For the SHERPA ZZ and WZ simulation samples, a dilepton mass filter is applied, where the invariant mass of charged lepton pair (ee, $\mu\mu$, or $\tau\tau$) is required to be larger than 4 GeV. The MC@NLO [16] generator is used to model WW, $t\bar{t}$, Wt, and s-channel single top quark production. AcerMC [17] models t-channel single top quark production. Inclusive W and Z/γ^* production are simulated with Alpgen [18]. The POWHEG and SHERPA generators are also used to simulate Z/γ^* production. For the ZZ and WZ backgrounds, the MC prediction is used to estimate the background contribution, otherwise the simulation is used to cross-check data driven background estimates. In order to investigate the contributions from $H \to WW \to \ell\nu\ell\nu$ and $H \to ZZ \to \ell\ell\nu\nu$ for a 125 GeV SM Higgs boson, the simulation samples are generated with POWHEG interfaced with PYTHIA [19] showering. Table 1 shows the list of the MC simulation samples used to estimate the ZZ, WZ background and yields of the Standard Model Higgs boson processes sharing the same final state.

Background	Generator	Cross section	MC Statistics
ZZ inclusive	HERWIG	6.49 pb (7 TeV)	250k
$ZZ \to \ell\ell\nu\nu$	SHERPA	0.38 pb (8 TeV, $m_{\ell\ell}$-filtered)	400k
WZ inclusive	HERWIG	17.9 pb (7 TeV)	100k
$WZ \to \ell\nu\ell\ell$	SHERPA	2.51 pb (8 TeV, $m_{\ell\ell}$-filtered)	590k
$H \to ZZ^{(*)} \to \ell\ell\nu\nu$	POWHEG	16.3 fb (7 TeV)	50k
	POWHEG	20.8 fb (8 TeV)	50k
$H \to WW^{(*)} \to \ell\nu\ell\nu$	POWHEG	374.7 fb (7 TeV)	50k, 30k
	POWHEG	478.5 fb (8 TeV)	500k, 500k

Table 1: The MC simulation samples used to estimate the ZZ, WZ background, and yields of the Standard Model Higgs boson processes sharing the same final state. For the MC statistics of the $H \to WW^{(*)} \to \ell\nu\ell\nu$ boson samples, the first number indicates the statistics of the gluon-gluon fusion samples, whereas the second indicates the statistics of vector-boson fusion samples.

4 The ATLAS Detector

The ATLAS detector [20] is a multi-purpose particle physics detector with forward-backward symmetric cylindrical geometry[1]. The inner tracking detector covers a pseudorapidity of $|\eta| < 2.5$ and consists of a silicon pixel detector, a silicon microstrip detector, and a straw-tube transition radiation tracker. The inner tracking detector is surrounded by a thin superconducting solenoid providing a 2 T axial magnetic field. A high-granularity lead/liquid-argon (LAr) sampling calorimeter measures the energy and the position of electromagnetic showers with $|\eta| < 3.2$. An iron/scintillating-tile calorimeter measures hadronic showers in the central region ($|\eta| < 1.7$). The end-cap ($1.5 < |\eta| < 3.2$) and forward ($3.1 < |\eta| < 4.9$) regions are instrumented with LAr sampling calorimeters for measuring both the electromagnetic and hadronic showers. The muon spectrometer surrounds the calorimeters and consists of three large superconducting air-core toroids, each with eight coils, a system of precision tracking chambers ($|\eta| < 2.7$), and fast tracking chambers for triggering ($|\eta| < 2.4$). A three-level trigger systemselects events to be recorded for offline analysis.

5 Object Reconstruction

Electron candidates are reconstructed from narrow energy deposits in the electromagnetic calorimeter matched to inner detector tracks. In the 2012 data taking period and the associated detector simulation, electron tracks are refit using a Gaussian Sum Filter [21] to account for energy loss due to bremsstrahlung as the electron passes through the inner detector material. Identification criteria select electrons with 95% efficiency and with a jet rejection factor of approximately 5000 [22]. These identification criteria apply cuts on the calorimeter shower shape, the track quality and require a good spatial match between the track and calorimeter shower. Electrons are required to have transverse momentum, p_{T}, over 20 GeV for signal events and electrons having $p_{\mathrm{T}} > 7$ GeV with looser identification criteria are used to veto events having additional leptons. Identified electrons must satisfy $|\eta| < 2.47$. Electrons are required to be isolated from nearby tracks by requiring that the scalar sum of the p_{T} of tracks within a cone of radius $\Delta R = \sqrt{\Delta\eta^2 + \Delta\phi^2} = 0.2$ is no more than 10% of the electron p_{T}. Electrons are required to be separated

[1] ATLAS uses a right-handed coordinate system with its origin at the nominal interaction point. The z-axis is along the beam pipe, the x-axis points to the center of the LHC ring and the y-axis points upward. Cylindrical coordinates (r,ϕ) are used in the transverse plane, ϕ being the azimuthal angle around the beam pipe. The pseudorapidity η is defined as $\eta = -\ln[\tan(\theta/2)]$ where θ is the polar angle.

from identified muons by more than $\Delta R = 0.2$ and to be separated from identified jets by more than $\Delta R = 0.4$ excluding the inner cone of $\Delta R = 0.2$ where the jet is instead removed.

Muon candidates are reconstructed using a statistical combination of muon spectrometer and inner detector tracks [23]. The measured energy that the muon loses as it passes through the calorimeter is taken into account. Muons are required to have $p_{\mathrm{T}} > 20$ GeV and $|\eta| < 2.4$ for signal events. Muons having $p_{\mathrm{T}} > 7$ GeV are used to veto events having more than two leptons. Muons are required to be isolated from nearby tracks by requiring that the scalar sum of the p_{T} of tracks within a cone of radius $\Delta R = 0.2$ is no more than 10% of the muon p_{T}. Muons must be be separated from identified jets by more than $\Delta R = 0.4$.

The trigger and identification efficiencies of electrons and muons are determined from high statistics Z boson samples. Scale factors within 5% of unity are applied to the simulation to correct these efficiencies to agree with data. The lepton momentum resolutions are also measured in high statistics Z boson samples and corrections are applied to the simulation.

Jets are reconstructed using the anti-k_t algorithm [24] using a distance parameter $R = 0.4$. Jets must have $p_{\mathrm{T}} > 20$ GeV and pseudorapidity of $|\eta| < 4.5$. To discriminate against jets from additional minimum bias interactions (pileup), the momentum fraction of tracks pointing to the jet area that originate from the highest $\sum p^2_{\mathrm{T,track}}$ vertex is required to be greater than 0.75 for the 2011 data taking period for jets inside the η-region with charged track particles. During the 2012 data taking period the cut is decreased to 0.5 in response to the presence of more pileup.

The $E_{\mathrm{T}}^{\mathrm{miss}}$ in ATLAS [25] is defined as the absolute amplitude of the vector sum of the momenta from calibrated objects, such as identified electrons, muons, photons, hadronic decays of tau leptons, and jets. Clusters of calorimeter cells that do not match any object are also included in the calculation. If an inner detector track matches such a calorimeter cluster the track momentum is used instead of the calorimeter measurement. The track-based missing transverse momentum ($\vec{p}_{\mathrm{T}}^{\mathrm{miss}}$) is also used along with the $E_{\mathrm{T}}^{\mathrm{miss}}$. The $\vec{p}_{\mathrm{T}}^{\mathrm{miss}}$ is computed from all the inner detector tracks having $p_{\mathrm{T}} > 500$ MeV and $|\eta| < 2.5$ that are consistent with having originated from the highest $\sum p^2_{\mathrm{T,track}}$ vertex and pass track quality criteria [26]. The momentum of a track matched to an electron is replaced by the more accurate measurement of the electron cluster transverse energy.

6 Event Selection

Events are selected using a combination of triggers that select single electrons or muons or a pair of electrons or muons as mentioned in Section 3. Events are further pre-selected by requiring that at least one reconstructed vertex has at least three associated tracks with $p_{\mathrm{T}} > 500$ MeV. This analysis is critically dependent upon the $E_{\mathrm{T}}^{\mathrm{miss}}$ performance, so overall data quality criteria are applied to reject events with non-collision backgrounds such as cosmic-ray muons and beam-related backgrounds, or events with degraded detector performance that can cause large mismeasurement of the $E_{\mathrm{T}}^{\mathrm{miss}}$ [27].

Events must have exactly two opposite-charge electrons or muons having $p_{\mathrm{T}} > 20$ GeV. To reduce the background from WZ events where the lepton originating from the W decay has $p_{\mathrm{T}} < 20$ GeV, events are removed if an additional electron or muon is reconstructed with $p_{\mathrm{T}} > 7$ GeV. The invariant mass of the dilepton system ($m_{\ell\ell}$) is required to satisfy 76 GeV $< m_{\ell\ell} <$ 106 GeV to be consistent with leptons from a Z boson.

Figure 2 shows the $E_{\mathrm{T}}^{\mathrm{miss}}$ distributions after the dilepton mass requirement. The data agree with the MC within the uncertainty error bands. To reject the majority of the Z background the $E_{\mathrm{T}}^{\mathrm{miss}}$ is required to be greater than 90 GeV. In events having true $E_{\mathrm{T}}^{\mathrm{miss}}$ originating from weakly interacting particles, such as neutrinos escaping the detector, the $\vec{p}_{\mathrm{T}}^{\mathrm{miss}}$ will be oriented in the same direction in azimuth as the $E_{\mathrm{T}}^{\mathrm{miss}}$ vector. Therefore the azimuthal difference of these two vectors ($\Delta\phi(E_{\mathrm{T}}^{\mathrm{miss}}, \vec{p}_{\mathrm{T}}^{\mathrm{miss}})$) is required to be less than 0.2 radians. The distribution of $\Delta\phi(E_{\mathrm{T}}^{\mathrm{miss}}, \vec{p}_{\mathrm{T}}^{\mathrm{miss}})$ in the 2012 data, after the dilepton mass window

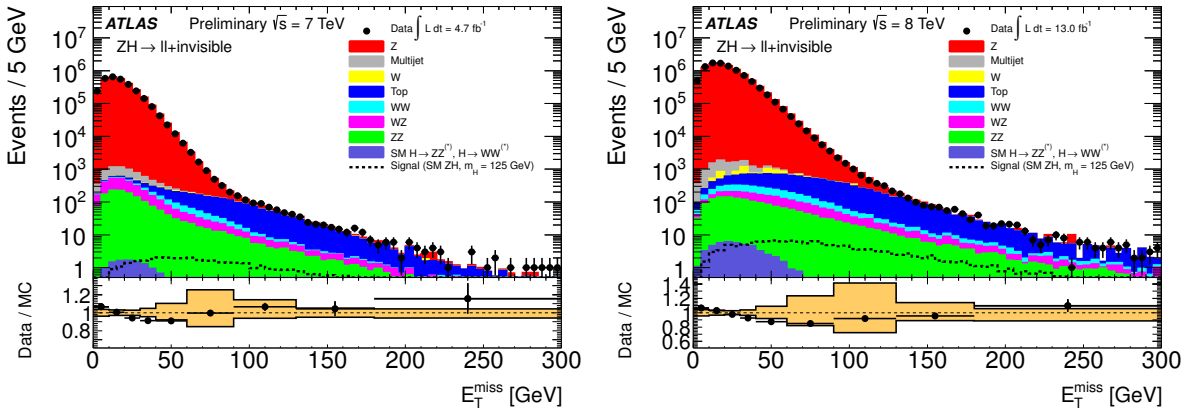

(a) (b)

Figure 2: $E_{\mathrm{T}}^{\mathrm{miss}}$ distributions after the dilepton mass requirement from the 2011 (a) and 2012 (b) data. The observed data are represented by the black dots and the histograms represent the background predictions from the MC samples listed in Section 3. The signal hypothesis is shown by the dotted line and assumes the SM ZH production rate for a Higgs boson with $m_H = 125$ GeV and a 100% invisible branching fraction. The insets at the bottom of the figures show the ratio of the data to the combined background expectations as well as a band corresponding to the combined systematic uncertainties.

requirement and $E_{\mathrm{T}}^{\mathrm{miss}}$ cut, is shown in Figure 3(a).

Under the signal assumption, the momentum of the reconstructed Z boson is balanced by the momentum of the invisibly decaying Higgs boson which is reconstructed as $E_{\mathrm{T}}^{\mathrm{miss}}$. Therefore the azimuthal separation between the dilepton system and the $E_{\mathrm{T}}^{\mathrm{miss}}$ ($\Delta\phi_{Z,E_{\mathrm{T}}^{\mathrm{miss}}}$) is required to be greater than 2.6 radians. The distribution of $\Delta\phi_{Z,E_{\mathrm{T}}^{\mathrm{miss}}}$ in the 2012 data, after the dilepton mass window requirement and $E_{\mathrm{T}}^{\mathrm{miss}}$ cut, is shown in Figure 3(b). In order to produce the required large $E_{\mathrm{T}}^{\mathrm{miss}}$, the Higgs boson must have a large p_{T} boost and therefore the recoiling Z boson must also have large p_{T} to conserve momentum. This causes the decay leptons to be close in azimuth and therefore the azimuthal opening angle of the two leptons ($\Delta\phi_{\ell\ell}$) is required to be less than 1.7 radians. Furthermore the magnitude of $p_{\mathrm{T}}^{\ell\ell}$ and $E_{\mathrm{T}}^{\mathrm{miss}}$ should be compatible and thus the fractional p_{T} difference, defined as $|E_{\mathrm{T}}^{\mathrm{miss}} - p_{\mathrm{T}}^{\ell\ell}|/p_{\mathrm{T}}^{\ell\ell}$, is required to be less than 0.2. The distribution of $|E_{\mathrm{T}}^{\mathrm{miss}} - p_{\mathrm{T}}^{\ell\ell}|/p_{\mathrm{T}}^{\ell\ell}$ in the 2012 data, after the dilepton mass window requirement and $E_{\mathrm{T}}^{\mathrm{miss}}$ cut, is shown in Figure 3(c). Finally, a majority of the signal is produced in association with no high p_{T} jets whereas background from boosted Z bosons and $t\bar{t}$ pairs tends to have one or more jets. Thus, events must have no reconstructed jets with $p_{\mathrm{T}} > 20$ GeV and $|\eta| < 2.5$. The distribution of the number of jets per event in the 2012 data after the dilepton mass window requirement and $E_{\mathrm{T}}^{\mathrm{miss}}$ cut, is shown in Figure 3(d).

7 Control Regions and Background Estimation

The processes that contribute to the SM expectation are summarized in Section 2. Table 3 summarizes the expected contributions from each background source and observed number of data events.

The ZZ [28] and WZ [29] backgrounds are estimated using MC predictions. The $ZZ \to \ell\ell\nu\nu$ and the $WZ \to \ell\nu\ell\ell$ MC are normalized to NLO cross sections. The cross section of the ZZ process is increased by 6% [30] to account for missing quark-box diagrams ($gg \to ZZ$). Systematic uncertainties are derived from the propagation of reconstructed object uncertainties and from uncertainties on the production cross

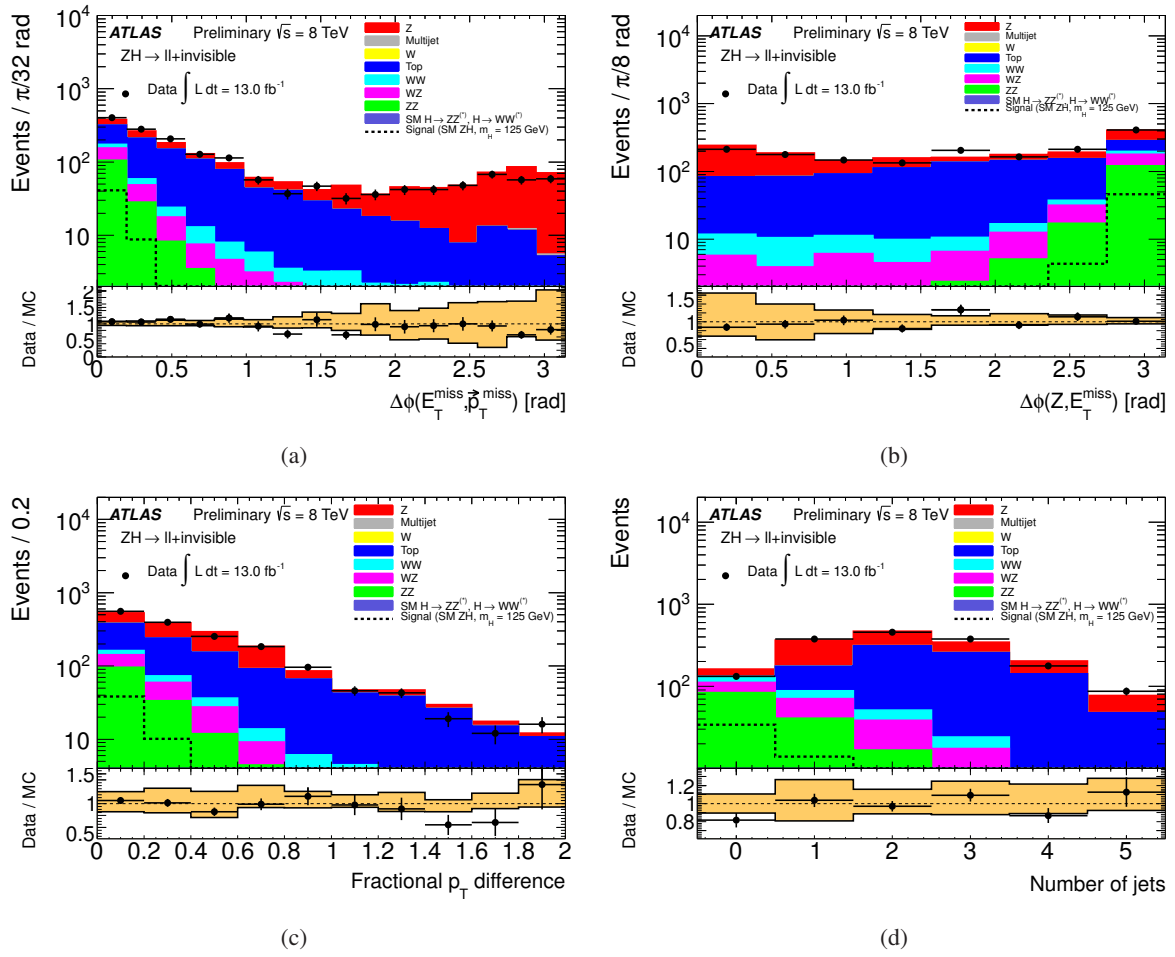

Figure 3: The distribution of $\Delta\phi(E_{\mathrm{T}}^{\mathrm{miss}}, \vec{p}_{\mathrm{T}}^{\mathrm{miss}})$ (a), $\Delta\phi_{Z,E_{\mathrm{T}}^{\mathrm{miss}}}$(b), $|E_{\mathrm{T}}^{\mathrm{miss}} - p_{\mathrm{T}}^{\ell\ell}|/p_{\mathrm{T}}^{\ell\ell}$ (c) and the number of selected jets (d) for events passing the dilepton mass requirement and $E_{\mathrm{T}}^{\mathrm{miss}}$ cut in the 2012 analysis. The observed data are represented by the black dots and the histograms represent the background predictions from the Monte Carlo samples listed in Section 3. The signal hypothesis is shown by the dotted line and assumes the SM ZH production rate for a Higgs boson with $m_H = 125$ GeV and a 100% invisible branching fraction. The insets at the bottom of the figures show the ratio of the data to the combined background expectations as well as a band corresponding to the combined systematic uncertainties.

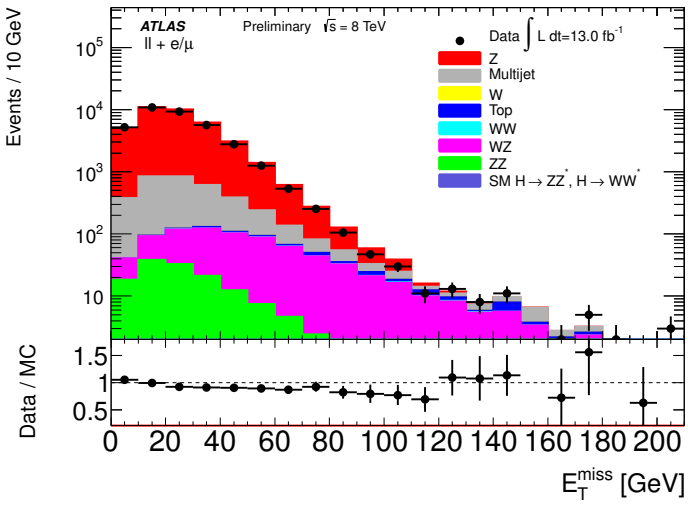

Figure 4: $E_{\mathrm{T}}^{\mathrm{miss}}$ distribution for data and MC events containing an oppositely charged electron or muon pair and an additional electron or muon.

section as described in Section 8. The total systematic uncertainty on these backgrounds is 11% in the 2011 data taking period and 10% in the 2012 data taking period. The MC simulation of the WZ events is validated in a trilepton control region as shown in Figure 4.

The contributions from WW, $t\bar{t}$, Wt, and $Z \to \tau\tau$ are estimated by exploiting the flavor symmetry in the final states of these processes. The branching fraction to the $e\mu$ final state is twice that of the ee or $\mu\mu$ final states. Therefore, the signal free $e\mu$ control region is used to extrapolate these backgrounds to the ee and $\mu\mu$ channels. Figure 5 shows the $E_{\mathrm{T}}^{\mathrm{miss}}$ distribution for data and MC events with the $e\mu$ final states from the 2012 dataset. The third lepton veto is applied, but no additional cut is applied in the figure. This method applies the signal selection to the $e\mu$ final state and corrects for differences between the identification efficiencies of electrons and muons using a Z control region as shown in Equation (1)-(3):

$$N_{ee}^{\mathrm{bkg}} = \frac{1}{2} \times N_{e\mu}^{\mathrm{data,sub}} \times k \tag{1}$$

$$N_{\mu\mu}^{\mathrm{bkg}} = \frac{1}{2} \times N_{e\mu}^{\mathrm{data,sub}} \times \frac{1}{k} \tag{2}$$

$$k = \sqrt{\frac{N_{ee}^{\mathrm{data}}}{N_{\mu\mu}^{\mathrm{data}}}} \tag{3}$$

N_{ee}^{bkg} and $N_{\mu\mu}^{\mathrm{bkg}}$ are the number of background events to be estimated per $E_{\mathrm{T}}^{\mathrm{miss}}$ bin, $N_{e\mu}^{\mathrm{data,sub}}$ is the number of events in the $e\mu$ control region with non-WW, $t\bar{t}$, Wt, and $Z \to \tau\tau$ backgrounds subtracted using MC simulation, k is a scale factor to correct for the differences in efficiency performance between electrons and muons given by Equation (3), and N_{ee}^{data} and $N_{\mu\mu}^{\mathrm{data}}$ are the number of dielectron and dimuon events after the Z mass window requirement in each $E_{\mathrm{T}}^{\mathrm{miss}}$ bin. The square root comes from the fact that the scale factor is derived from dilepton events, whereas the correction itself is only applied to one of the leptons. Important sources of systematic uncertainty are uncertainties in the MC used for the subtraction, and variations in the correction factor k. After the dilepton requirement and no additional cuts, the value of k is 0.97 from the MC, and 0.94 from the data. The maximum variation of the correction factor, observed at each cut level in the signal selection, is used to estimate the uncertainty. The differences in

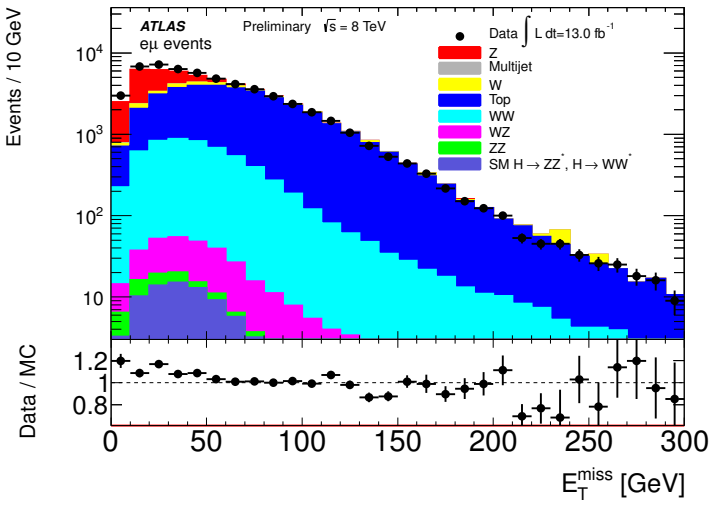

Figure 5: $E_{\mathrm{T}}^{\mathrm{miss}}$ distribution for data and MC events with the $e\mu$ final states from the 2012 dataset.

kinematics for the $e\mu$ and dielectron or dimuon events are also considered as systematics. The combined systematic uncertainty from MC subtraction and the maximum variation of the correction factor is 16% for the 2012 data. The estimated background from these sources is consistent with the expectation from the MC simulation within the uncertainty. As this data-driven estimate gives a consistent expectation, but with larger uncertainty for the 2011 data, the MC-driven estimates for WW, $t\bar{t}$, and single top quark events are used for the 2011 data. The Monte Carlo samples are validated in the $e\mu$ control region. The validation of the top quark MC samples is shown in Figure 6 in the $e\mu$ final states with a b-tagged jet [31] in the events.

The background from inclusive Z boson production is estimated using the so called $ABCD$ method utilizing four regions (the signal region A and three side-band regions B-D) formed by two uncorrelated variables: the $\Delta\phi(E_{\mathrm{T}}^{\mathrm{miss}}, \vec{p}_{\mathrm{T}}^{\mathrm{miss}})$ and fractional p_{T} difference. The four regions are formed by either applying or reversing the cuts at the thresholds for these two variables as shown in Figure 7. Figure 8 shows the $E_{\mathrm{T}}^{\mathrm{miss}}$ distributions in Regions A-D after the dilepton mass requirement and jet veto for the 2012 data. The events in the signal region are estimated as follows:

$$N_A^{\mathrm{est}} = N_B^{\mathrm{obs}} \times \frac{N_C^{\mathrm{obs}}}{N_D^{\mathrm{obs}}} \times \alpha \tag{4}$$

where, N_A^{est} is the number of estimated Z background in the signal region, and N_X^{obs} is the number of observed events in Region X (X=B-D). Contributions from non-Z backgrounds in Regions B-D are subtracted before applying this equation. A small impact from the correlation between the two variables is considered in the correction factor α, which is 1.07 (1.04) for the 2011 (2012) data. A correction factor of less than 10% is derived from MC simulation. Systematic uncertainties are derived by evaluating the compatibility of the $E_{\mathrm{T}}^{\mathrm{miss}}$ distributions in the control regions and from the variation in the correction factor after the various selection requirements. The subtraction of non-Z backgrounds in Regions B-D is also considered as a source of systematic uncertainty. The total systematic uncertainty is 56% in the 2011 data and 51% in the 2012 data.

The background from inclusive W production and multijet events is estimated using the Matrix Method [32]. A 4×4 matrix is derived from the selection efficiencies of nominally selected signal

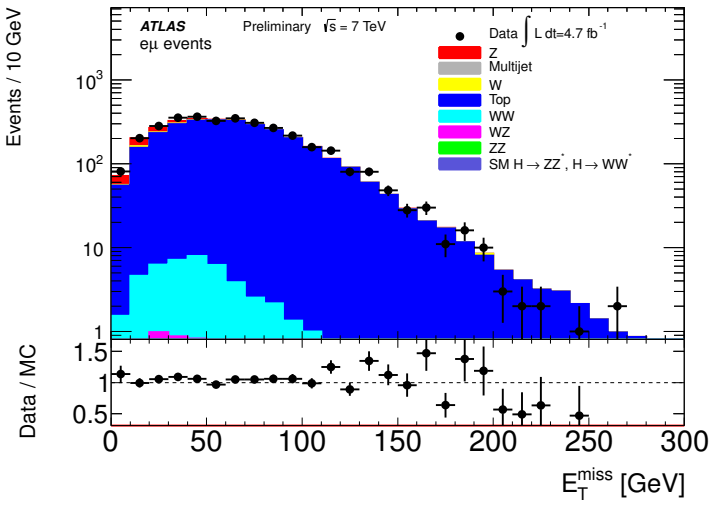

Figure 6: $E_{\mathrm{T}}^{\mathrm{miss}}$ distribution for data and MC events with the $e\mu$ final states from the 2011 dataset with a b-tagged jet.

leptons (T) and rejection probabilities of a loosened lepton (L) definition as shown in Equation (5).

$$\begin{bmatrix} N_{TT} \\ N_{TL} \\ N_{LT} \\ N_{LL} \end{bmatrix} = \begin{bmatrix} r_1 r_2 & r_1 f_2 & f_1 r_2 & f_1 f_2 \\ r_1(1-r_2) & r_1(1-f_2) & f_1(1-r_2) & f_1(1-f_2) \\ (1-r_1) r_2 & (1-r_1) f_2 & (1-f_1) r_2 & (1-f_1) f_2 \\ (1-r_1)(1-r_2) & (1-r_1)(1-f_2) & (1-f_1)(1-r_2) & (1-f_1)(1-f_2) \end{bmatrix} \times \begin{bmatrix} N_{RR} \\ N_{RF} \\ N_{FR} \\ N_{FF} \end{bmatrix}. \quad (5)$$

N_{TT} is the number of events which has exactly two leptons passing nominal criteria defined in Section 5, N_{TL} and N_{LT} is the number of events which has only one lepton that passes the nominal criteria, N_{LL} is the number of events which have exactly two leptons that pass looser cuts but do not pass the nominal cuts. For electrons, "L" corresponds to electrons with looser identification criteria and the isolation cut not being applied. For muons, "L" corresponds to muons with all the nominal cuts applied but the isolation cut. N_{RR} means the number of events which has exactly two "real" leptons, N_{RF} and N_{FR} means the number of events which has only one "real" lepton and one "fake" lepton, N_{FF} means the number of events which has exactly two "fake" leptons. The r_1, r_2, f_1, f_2 are lepton efficiencies and fake rates for the first lepton and the second lepton, respectively. The lepton efficiency (fake rate) is the ratio between the number of real (fake) leptons passing the "Tight" cut and the corresponding number of leptons passing the "Loose" cuts. The efficiency and fake rate depend on lepton transverse momentum p_T. The matrix transforms the measured rate of events containing two signal leptons, one signal lepton and one loose lepton, or two loose leptons to the desired rate of events where two real leptons, one real and one fake lepton, or two fake leptons are produced. The W and multijet background is estimated as below:

$$N_{W+\mathrm{jets}} = \sum_{i}^{N_{\mathrm{events}}} N_{RF}^{i} \times r_1^{i} \times f_2^{i} + N_{FR}^{i} \times f_1^{i} \times r_2^{i}, \quad (6)$$

$$N_{\mathrm{multijet}} = \sum_{i}^{N_{\mathrm{events}}} N_{FF}^{i} \times f_1^{i} \times f_2^{i}. \quad (7)$$

Systematic uncertainties are dominated by the measurement of the lepton fake rates. The selection requirements that define the sample from which the fake rates are derived are varied and the deviations in

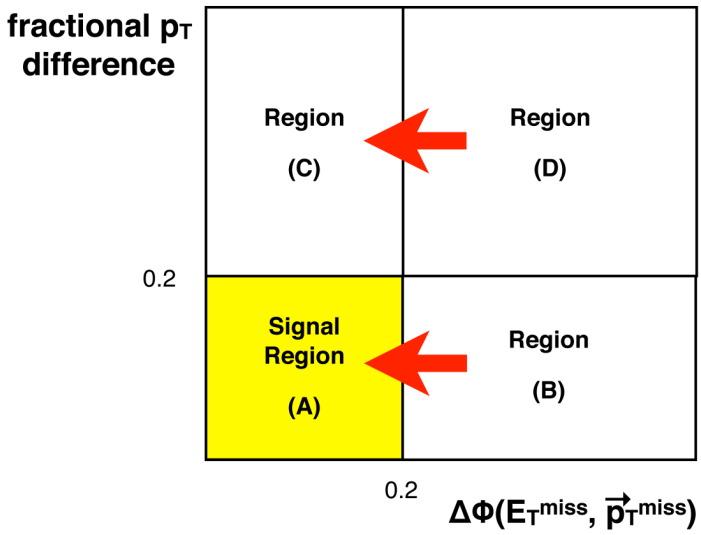

Figure 7: Regions A-D formed by $\Delta\phi(E_{\mathrm{T}}^{\mathrm{miss}}, \vec{p}_{\mathrm{T}}^{\mathrm{miss}})$ and fractional p_{T} difference variables.

the obtained results are taken as the systematic uncertainties. This yields an uncertainty of 15% in the 2011 data and 22% in the 2012 data.

8 Systematic Uncertainties

Systematic uncertainties on individual data driven background estimates are described in section 7. Table 2 summarizes the systematic uncertainties estimated in this analysis.

Systematic uncertainties on the signal model, the ZZ and WZ backgrounds are estimated from MC samples. The WW and top quark backgrounds are also estimated from MC samples for 2011. Uncertainties on backgrounds that are either measured from data, or based on normalization to data in control regions, take into account systematic effects associated to the methods and the control samples considered. The luminosity uncertainty is 1.8% for the 2011 data taking period [33] and 3.6% for the 2012 data taking period. The luminosity uncertainty for the 2012 data is derived, following the same methodology as that detailed in [33], from a preliminary calibration of the luminosity scale derived from beam-separation scans performed in April 2012. Lepton trigger and identification efficiencies as well as energy scale and resolution uncertainties are derived from high statistics Z samples. Propagated to the event selection, these uncertainties contribute typically 1.0-1.5% to the overall selection uncertainty in the signal and backgrounds estimated from the MC simulation. Jet energy scale and resolution uncertainties are derived using a combination of techniques that use dijet, photon + jet, and Z + jet events [34]. The impact of these jet uncertainties on the jet veto is also considered. These uncertainties contribute a 3%-6% uncertainty to the final event selection. Both the uncertainties on the leptons and those on the jets are propagated to the $E_{\mathrm{T}}^{\mathrm{miss}}$ calculation, and the resulting uncertainty on the latter is thus included in the selection uncertainties given above. An additional uncertainty on $E_{\mathrm{T}}^{\mathrm{miss}}$ related to uncertainties in the pile-up simulation contribute a 1%-2% uncertainty on the final event selection in signal and backgrounds estimated from the MC simulation.

Uncertainties on the ZH production cross section are derived from variations of the QCD scale, α_s and PDF variations [7, 8] combined to give an uncertainty of 4.9-5.1% on the cross section for the SM Higgs boson having a mass between 115 and 300 GeV. This analysis is sensitive to the simulation of the

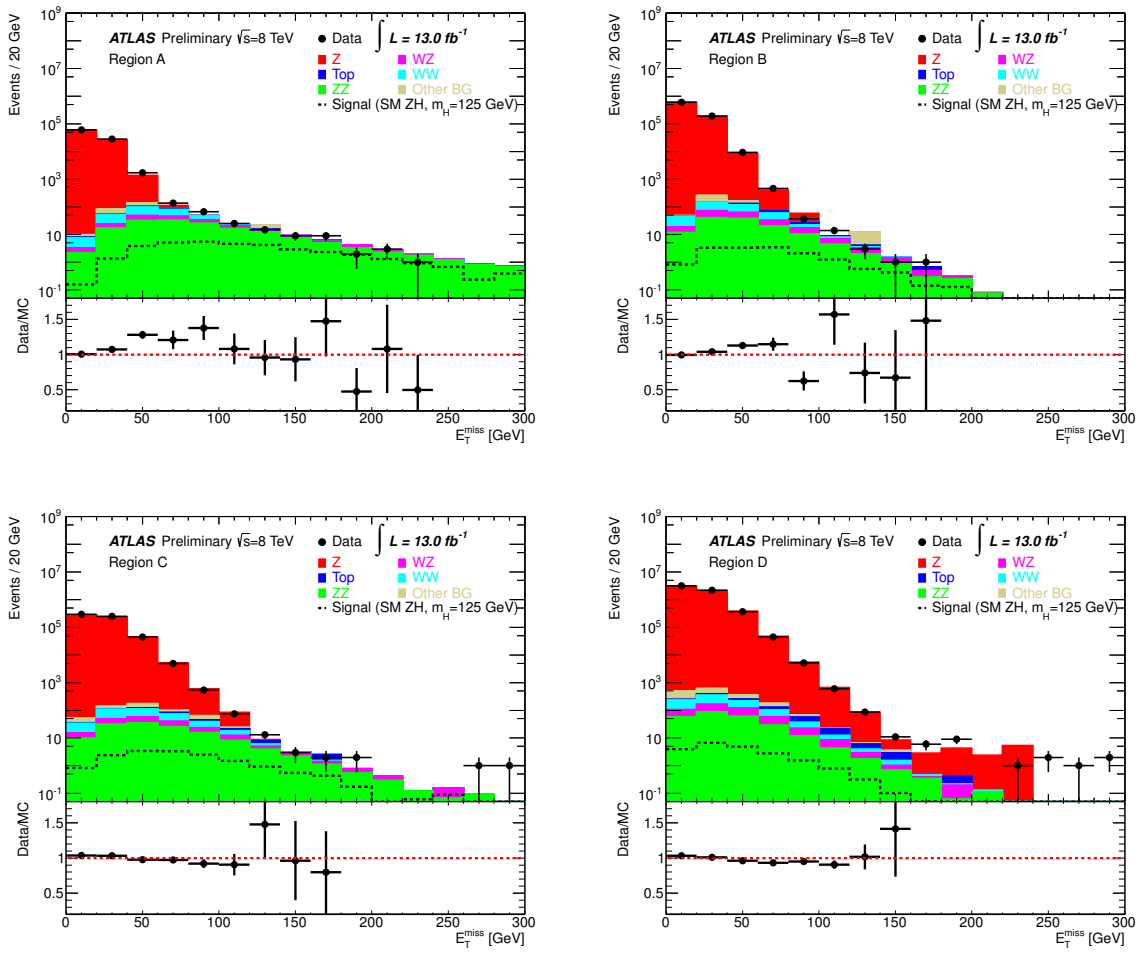

Figure 8: $E_{\mathrm{T}}^{\mathrm{miss}}$ distribution for data and MC events in Regions A-D after the dilepton mass requirement and jet veto for the 2012 data. The signal region A and three side-band regions B-D are formed by applying or reversing cuts with the two uncorrelated variables: the $\Delta\phi(E_{\mathrm{T}}^{\mathrm{miss}}, \vec{p}_{\mathrm{T}}^{\mathrm{miss}})$ and fractional p_{T} difference.

Higgs boson p_{T} through the $E_{\mathrm{T}}^{\mathrm{miss}}$, and uncertainties in the p_{T} boost of the Higgs boson can affect the signal yield. Currently, an additional systematic uncertainty of 1.9% is applied to the normalization [35, 36], and differential uncertainties as a function of the Higgs boson p_T is considered as shape systematics.

The normalization uncertainty on the background Monte Carlo used to estimate the ZZ background is 6% from varying the PDF, α_S, and QCD scale. Such theoretical uncertainty on the jet veto is estimated as 0.7% (0.8%) for 2011 (2012) in the diboson events from generator studies. The impact of PDF, α_S, and QCD scale uncertainties on the shape of the $E_{\mathrm{T}}^{\mathrm{miss}}$ distributions is also considered [8]. The effects of missing quark-box diagrams ($gg \to ZZ$) as mentioned in Section 7 is also considered as systematics of 6% as the same size of the cross section rescaling. The theoretical uncertainty of the WZ and WW background is considered similarly.

The object and theoretical uncertainties are considered as correlated between the 2011 and 2012 data, and between the signals and all the backgrounds estimated from the MC simulation. The systematic uncertainties in the data-driven methods are also assumed to be correlated between the two datasets. The

Process	Estimation method	Uncertainty (%)	
		2011	2012
ZH Signal	MC	7	6
ZZ	MC	11	10
WZ	MC	12	14
WW	MC	14	not used
Top quark	MC	90	not used
Top quark, WW and $Z \to \tau\tau$	$e\mu$ CR	not used	4
Z	ABCD method	56	51
W + jets, multijet	Matrix method	15	22

Table 2: Summary of the systematic uncertainties on each background and on the signal yield. The method used to estimate the backgrounds and the associated sources of systematic uncertainties are given. The total systematic uncertainties for each data taking period are given.

Data Period	2011 (7 TeV)	2012 (8 TeV)
ZZ	$23.5 \pm 0.8 \pm 2.5$	$56.5 \pm 1.2 \pm 5.7$
WZ	$6.2 \pm 0.4 \pm 0.7$	$13.9 \pm 1.2 \pm 2.1$
WW	$1.1 \pm 0.2 \pm 0.2$	used $e\mu$ data-driven
Top quark	$0.4 \pm 0.1 \pm 0.4$	used $e\mu$ data-driven
Top quark, WW and $Z \to \tau\tau$ ($e\mu$ data-driven)	used MC	$4.9 \pm 0.9 \pm 0.2$
Z	$0.16 \pm 0.13 \pm 0.09$	$1.4 \pm 0.4 \pm 0.7$
W + jets, multijet	$1.3 \pm 0.3 \pm 0.2$	$1.4 \pm 0.4 \pm 0.3$
Total BG	$32.7 \pm 1.0 \pm 2.6$	$78.0 \pm 2.0 \pm 6.5$
Observed	27	71

Table 3: Observed number of events and expected contributions from each background source separated into the 2011 and 2012 data taking periods. Uncertainties associated with the background predictions are presented with the statistical uncertainty first and the systematic uncertainty second.

luminosity uncertainty is considered as uncorrelated between the 2011 and 2012 data. The uncertainties for the WW and top quark backgrounds are considered as uncorrelated between the 2011 and 2012 data, as different methods are used for the background estimation between the two datasets.

9 Results

The number of observed and expected events for both the 2011 and 2012 data taking periods are shown in Table 3. Figure 9 shows the final $E_{\mathrm{T}}^{\mathrm{miss}}$ distribution with the observed data and expected backgrounds for the 2011 and 2012 data taking periods. In Figure 9, the signal model assumes a SM ZH production rate for a Higgs boson with $m_H = 125$ GeV and a 100% branching fraction to invisible particles. No excess is observed over the SM expectation and limits are set for two scenarios for invisibly decaying Higgs-like bosons. The first scenario explores the possibility that the recently observed Higgs-like boson with mass around 125 GeV has a non-negligible branching ratio to invisible particles, well beyond that expected in SM. The second scenario considers the possibility of a Higgs-like boson in a range of masses from $m_H = 115$ GeV to $m_H = 300$ GeV with a significant branching fraction to invisible particles.

The limits are computed from a maximum likelihood fit to the $E_{\mathrm{T}}^{\mathrm{miss}}$ distribution following the CL_s modified frequentist formalism [37] with the profile likelihood test statistic [38].

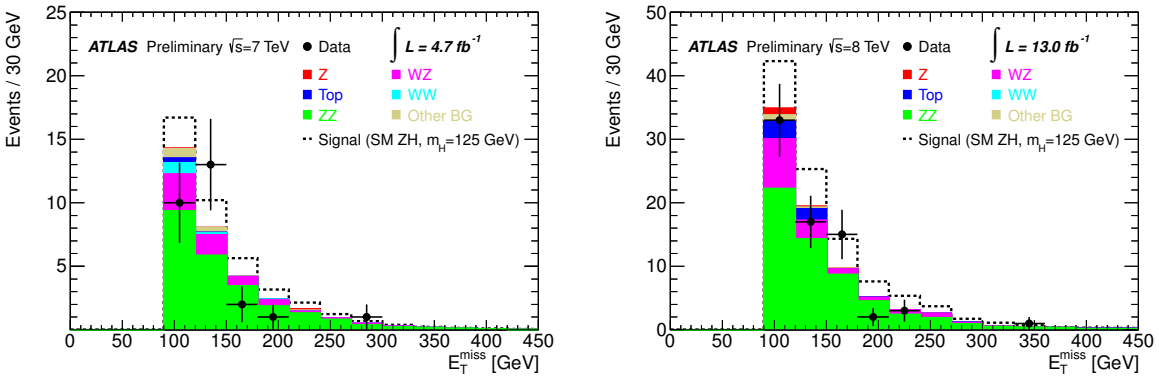

(a) (b)

Figure 9: Distributions of $E_{\mathrm{T}}^{\mathrm{miss}}$ for signal events in the 2011 data taking period (a) and the 2012 data taking period (b). The observed data are indicated by the black points and the histograms represent the background predictions. The dashed line indicates the prediction from the signal model and is stacked on the background prediction. The signal model assumes a SM Higgs boson having a mass of 125 GeV and a 100% branching fraction to invisible particles.

Figure 10 shows the interpretation in the first scenario, where the recently observed Higgs-like boson around 125 GeV decays invisibly. The confidence level (CL) is plotted against the BR($H \rightarrow$ invisible). Red lines indicate the 68% and 95% CL. Assuming the ZH production rate for a 125 GeV SM Higgs boson, limits are set on the invisible branching fraction at 95% confidence level. The observed exclusion is for branching fractions greater than 65%, and the expected limit is 84%.

For the second scenario, where a Higgs-like boson with a significant branching fraction to invisible particles exists in the mass range of 115 GeV to 300 GeV, limits are set considering only the hypothesis of a single invisibly decaying Higgs-like boson. Thus the limits do not consider possible multiple Higgs boson candidates, including the 125 GeV candidate state, all having non-negligible invisible branching fractions. Figure 11 shows 95% confidence level limits on the ZH production cross section multiplied by the invisible branching fraction of such a Higgs boson in the mass range $m_H = 115$ GeV to $m_H = 300$ GeV for the considered data taking periods in 2011 and 2012, as well as the limit achieved from the combination of both periods. No excess is observed over the mass range.

10 Summary and Conclusion

A direct search for evidence of invisible decays of a Higgs boson at the LHC has been performed. While the invisible branching fraction for a SM Higgs boson is too small to be accessible, this measurement is sensitive to enhancements of the invisible branching fraction, such as from decays to dark matter particles. After the full selection, 27 events are observed compared to a SM expectation of 32.7 ± 1.0 (stat.) ± 2.6 (syst.) background events in 4.7 fb^{-1} of data taken at $\sqrt{s} = 7$ TeV during the 2011 run and 71 events are observed compared to an expected 78.0 ± 2.0 (stat.) ± 6.5 (syst.) background events in 13.0 fb^{-1} of data taken at $\sqrt{s} = 8$ TeV during part of the 2012 run. No significant excess over the expected background is observed and limits are set on the allowed invisible branching fraction of the recently observed 125 GeV Higgs boson candidate. Assuming the ZH production rate for a 125 GeV SM Higgs boson, limits are set on the invisible branching fraction at 95% confidence level. The observed exclusion is for branching fractions greater than 65%, and the expected limit is 84%. Limits are also set

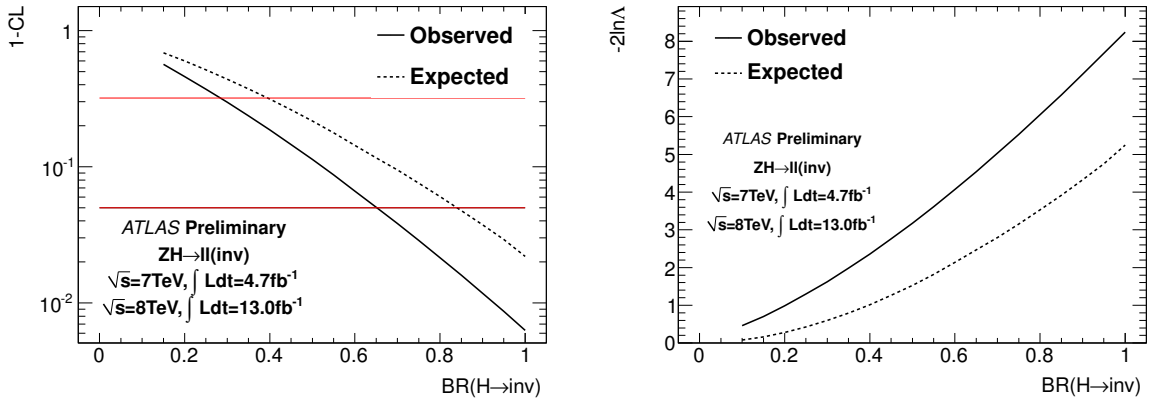

Figure 10: 1 - Confidence level (CL) (a) and profile likelihood (b) scanned against BR($H \rightarrow$ invisible) for the SM Higgs boson with 125 GeV mass. The dashed line shows the expected values, whereas the solid line indicates the observed values. The red solid lines indicate the 68% and 95% CL for (a).

on the cross section times invisible branching fraction of a possible additional Higgs-like boson over the mass range 115 GeV $< m_H <$ 300 GeV. No excess is observed over the mass range.

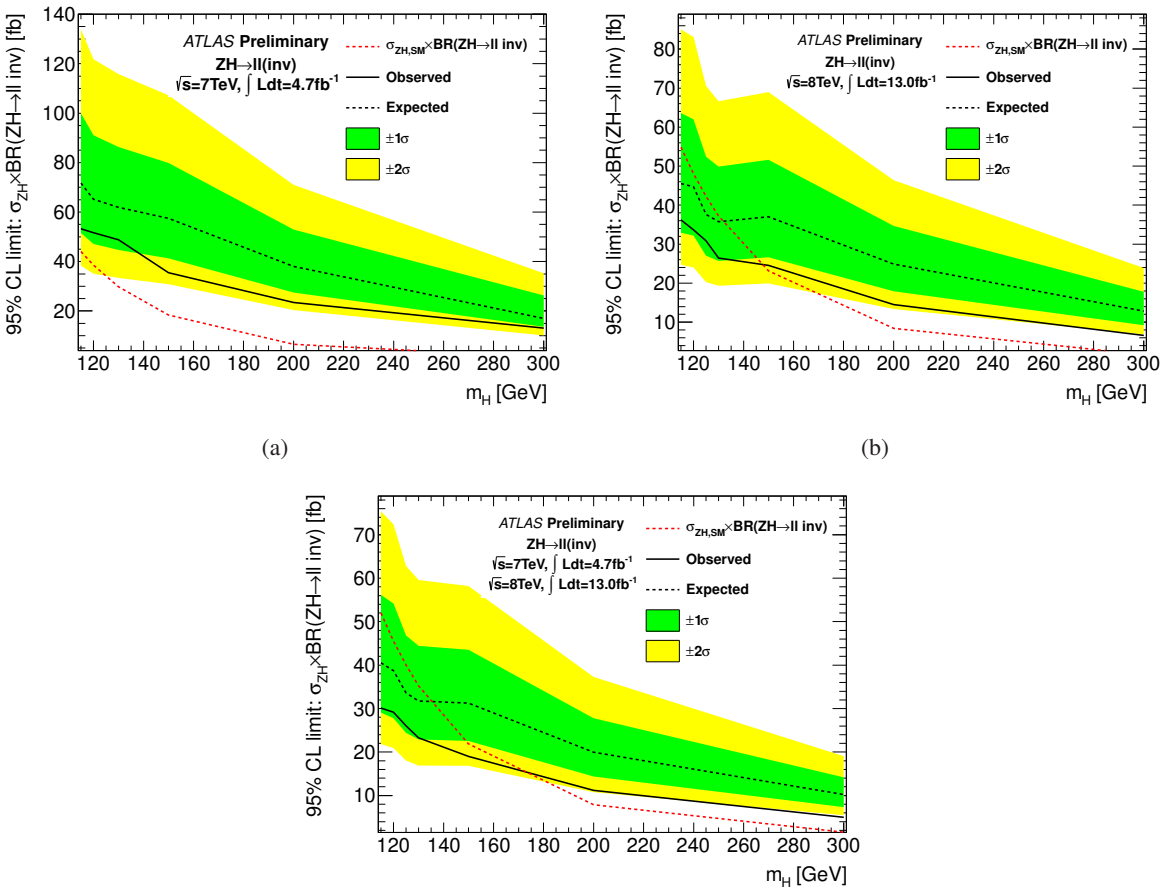

(a) (b)

(c)

Figure 11: 95% confidence level limits on the cross section times branching fraction of a Higgs-like boson decaying to invisible particles for the 2011 data taking period (a), 2012 data taking period (b), and combination of both periods (c). Dashed lines show the background only expected limits and solid lines show the observed limit.

References

[1] F. Englert and R. Brout, *Broken symmetry and the mass of gauge vector mesons*, Phys. Rev. Lett. **13** (1964) 321–323.

[2] P. W. Higgs, *Broken symmetries and the masses of gauge bosons*, Phys. Rev. Lett. **13** (1964) 508–509.

[3] G. Guralnik, C. Hagen, and T. Kibble, *Global conservation laws and massless particles*, Phys. Rev. Lett. **13** (1964) 585–587.

[4] ATLAS Collaboration, *Observation of a new particle in the search for the Standard Model Higgs boson with the ATLAS detector at the LHC*, Phys. Lett. **B716** (2012) 1–29, arXiv:1207.7214 [hep-ex].

[5] CMS Collaboration, *Observation of a new boson at a mass of 125 GeV with the CMS experiment at the LHC*, Phys. Lett. **B716** (2012) 30–61, arXiv:1207.7235 [hep-ex].

[6] LEP Higgs Working Group, *Searches for Invisible Higgs bosons: Preliminary combined results using LEP data collected at energies up to 209 GeV*, LHWG Note 2001-06 (2001), arXiv:hep-ex/0107032.

[7] LHC Higgs Cross Section Working Group, S. Dittmaier, C. Mariotti, G. Passarino, and R. Tanaka (Eds.), *Handbook of LHC Higgs Cross Sections: 1. Inclusive Observables*, CERN-2011-002 (CERN, Geneva, 2011), arXiv:1101.0593 [hep-ph].

[8] LHC Higgs Cross Section Working Group, S. Dittmaier, C. Mariotti, G. Passarino, and R. Tanaka (Eds.), *Handbook of LHC Higgs Cross Sections: 2. Differential Distributions*, CERN-2012-002 (CERN, Geneva, 2012), arXiv:1201.3084 [hep-ph].

[9] T. Han and S. Willenbrock, *QCD correction to the $pp \to WH$ and ZH total cross-sections*, Phys. Lett. **B273** (1991) 167–172.

[10] O. Brein, A. Djouadi, and R. Harlander, *NNLO QCD corrections to the Higgs-strahlung processes at hadron colliders*, Phys. Lett. **B579** (2004) 149–156, arXiv:hep-ph/0307206 [hep-ph].

[11] M. Ciccolini, S. Dittmaier, and M. Krämer, *Electroweak radiative corrections to associated WH and ZH production at hadron colliders*, Phys. Rev. **D68** (2003) 073003, arXiv:hep-ph/0306234 [hep-ph].

[12] S. Frixione, P. Nason and C. Oleari, *Matching NLO QCD computations with Parton Shower simulations: the POWHEG method*, JHEP **0711** (2007) 070, arXiv:0709.2092 [hep-ph].

[13] M. Bahr, S. Gieseke, M. A. Gigg, D. Grellscheid, K. Hamilton, O. Latunde-Dada, S. Platzer, P. Richardson, M. H. Seymour, A. Sherstnev, J. Tully, and B. R. Webber, *Herwig++ Physics and Manual*, Eur. Phys. J. C **58** (2008) 639–707, arXiv:0803.0883 [hep-ph].

[14] G. Corcella, I. Knowles, G. Marchesini, S. Moretti, K. Odagiri, P. Richardson, M. Seymour, and B. Webber, *HERWIG 6.5*, JHEP **0101** (2001) 010, arXiv:hep-ph/0011363.

[15] T. Gleisberg, S. Hoche, F. Krauss, M. Schonherr, S. Schumann, F. Siegert, and J. Winter, *Event generation with Sherpa 1.1*, JHEP **0902** (2009) 007, arXiv:0811.4622 [hep-ph].

[16] S. Frixione and B. R. Webber, *Matching NLO QCD computations and parton shower simulations*, JHEP **0206** (2002) 029.

[17] B. P. Kersevan and E. Richter-Was, *The Monte Carlo event generator AcerMC versions 2.0 to 3.8 with interfaces to PYTHIA 6.4, HERWIG 6.5 and ARIADNE 4.1*, Computer Physics Communications **184** no. 3, (2013) 919 – 985.

[18] M. L. Mangano, M. Moretti, F. Piccinini, R. Pittau and A. D. Polosa, *ALPGEN, a generator for hard multiparton processes in hadronic collisions*, JHEP **0307** (2003) 001, arXiv:hep-ph/0206293.

[19] T. Sjostrand, S. Mrenna and P. Z. Skands, *PYTHIA 6.4 Physics and Manual*, JHEP **0605** (2006) 026, arXiv:hep-ph/0603175.

[20] ATLAS Collaboration, *The ATLAS experiment at the CERN Large Hadron Collider*, JINST **3** (2008) S08003.

[21] ATLAS Collaboration, *Improved electron reconstruction in ATLAS using the Gaussian Sum Filter-based model for bremsstrahlung*, ATLAS-CONF-2012-047 (2012), https://cds.cern.ch/record/1449796.

[22] ATLAS Collaboration, *Electron performance measurements with the ATLAS detector using the 2010 LHC proton-proton collision data*, Eur. Phys. J. C **72** (2012) 1909, arXiv:1110.3174 [hep-ex].

[23] ATLAS Collaboration, *Expected performance of the ATLAS experiment - detector, trigger and physics*, CERN-OPEN-2008-020 (2009), arXiv:0901.0512 [hep-ex].

[24] M. Cacciari, G. P. Salam and G. Soyez, *The anti-k_t jet clustering algorithm*, JHEP **0804** (2008) 063, arXiv:0802.1189 [hep-ph].

[25] ATLAS Collaboration, *Performance of missing transverse momentum reconstruction in proton-proton collisions at $\sqrt{s}$ = 7 TeV with ATLAS*, Eur. Phys. J. C **72** (2012) 1844, arXiv:1108.5602 [hep-ex].

[26] ATLAS Collaboration, *Measurement of the missing transverse momentum based on tracks in proton-proton collisions at $\sqrt{s}$ =900 GeV centre-of-mass energy with the ATLAS detector*, ATLAS-CONF-2010-020 (2010), https://cds.cern.ch/record/1277652.

[27] ATLAS Collaboration, *Data-quality requirements and event cleaning for jets and missing transverse energy reconstruction with the ATLAS detector in proton-proton collisions at a center-of-mass energy of $\sqrt{s}$=7 TeV*, ATLAS-CONF-2010-038 (2010), https://cds.cern.ch/record/1277678.

[28] ATLAS Collaboration, *Measurement of the total ZZ production cross section in proton-proton collisions at $\sqrt{s}$ = 8 TeV in 20 fb^{-1} with the ATLAS detector*, to appear as ATLAS-CONF-2013-020.

[29] ATLAS Collaboration, *Measurement of WZ production in proton-proton collisions at $\sqrt{s}$ = 7 TeV with the ATLAS detector*, Eur. Phys. J. C **72** (2012), arXiv:1208.1390 [hep-ex].

[30] J.M. Campbell, R.K. Ellis, C. Williams, *Vector boson pair production at the LHC*, JHEP **07** (2011) 018.

[31] ATLAS Collaboration, *Commissioning of the ATLAS high-performance b-tagging algorithms in the 7 TeV collision data*, ATLAS-CONF-2011-102 (2011), https://cdsweb.cern.ch/record/1369219.

[32] ATLAS Collaboration, *Measurement of the top quark-pair production cross section with ATLAS in pp collisions at* $\sqrt{s}$ = 7 *TeV*, Eur. Phys. J. C **71** (2011) 1577.

[33] ATLAS Collaboration, *Improved luminosity determination in pp collisions at* $\sqrt{s}$ = 7 *TeV using the ATLAS Detector at the LHC*, CERN-PH-EP-2013-026 (2013), arXiv:1302.4393 [hep-ex].

[34] ATLAS Collaboration, *Jet energy scale and its systematic uncertainty in proton-proton collisions at* $\sqrt{s}$=7 *TeV with ATLAS 2011 data*, ATLAS-CONF-2013-004 (2013), https://cds.cern.ch/record/1509552.

[35] M. Ciccolini, A. Denner and S. Dittmaier, *Strong and electroweak corrections to the production of Higgs+2 jets via weak interactions at the LHC*, Phys. Rev. Lett. **99** (2007) 161803, arXiv:0707.0381 [hep-ph].

[36] ATLAS Collaboration, *Search for the Standard Model Higgs boson produced in association with a vector boson and decaying to bottom quarks with the ATLAS detector*, ATLAS-CONF-2012-161 (2012), https://cds.cern.ch/record/1493625.

[37] A.L. Read, *Presentation of search results: The CLs technique*, J. Phys. G **28** (2002) 2693–2704.

[38] G. Cowan, K. Cranmer, E. Gross, O. Vitells, *Asymptotic formulae for likelihood-based tests of new physics*, Eur. Phys. J. C **71** (2011) 1554.